

Query Adaptive Late Fusion for Image Retrieval

Zhongdao Wang, Liang Zheng, Shengjin Wang

Abstract—Feature fusion is a commonly used strategy in image retrieval tasks, which aggregates the matching responses of multiple visual features. Feasible sets of features can be either descriptors (SIFT, HSV) for an entire image or the same descriptor for different local parts (face, body). Ideally, the to-be-fused heterogeneous features are pre-assumed to be discriminative and complementary to each other. However, the effectiveness of different features varies dramatically according to different queries. That is to say, for some queries, a feature may be neither discriminative nor complementary to existing ones, while for other queries, the feature suffices. As a result, it is important to estimate the effectiveness of features in a query-adaptive manner. To this end, this article proposes a new late fusion scheme at the score level. We base our method on the observation that the sorted score curves contain patterns that describe their effectiveness. For example, an “L”-shaped curve indicates that the feature is discriminative while a gradually descending curve suggests a bad feature. As such, this paper introduces a query-adaptive late fusion pipeline. In the hand-crafted version, it can be an unsupervised approach to tasks like particular object retrieval. In the learning version, it can also be applied to supervised tasks like person recognition and pedestrian retrieval, based on a trainable neural module. Extensive experiments are conducted on two object retrieval datasets and one person recognition dataset. We show that our method is able to highlight the good features and suppress the bad ones, is resilient to distractor features, and achieves very competitive retrieval accuracy compared with the state of the art. In an additional person re-identification dataset, the application scope and limitation of the proposed method are studied.

Index Terms—Late fusion, particular object retrieval, person recognition, pedestrian retrieval.



1 INTRODUCTION

THIS paper considers the task of image retrieval, a critical task in computer vision. Given a query (probe) image, we aim at searching for all the true match images in a database (gallery). Relevant tasks include object retrieval that searches for the specific objects [12], [24], face/person recognition [7], [44] and pedestrian retrieval [29], [47], [50] that search for images with the same identity.

In these image retrieval tasks, there usually exist multiple complementary visual cues for measuring the similarity between images. For example, in particular object retrieval, popular choices include local descriptors like SIFT [22], and global descriptors like GIST [26]. For person recognition and re-identification, part-based features are often employed. The fusion of multiple features has been shown to provide multiple perspectives to describe images, pushing the retrieval accuracy forward. Typically, if a to-be-fused feature is moderately discriminative and complementary to existing features, it is expected that higher retrieval accuracy can be achieved after fusion.

There exist two mainstreams for multiple feature fusion: early fusion and late fusion. In early fusion, descriptors are combined at feature level [40] or even sensor level [30]. Then, the fused features are processed together through the learning pipeline. On the other hand, late fusion refers to fusion at score [45] or decision levels [14]. In late fusion, a good trade-off can be provided between the information content and the ease in fusion. This paper seeks to design a simple yet effective late fusion scheme which works on the

score level.

A major challenge in feature fusion is that a feature’s effectiveness is highly dependent on the query. Since different features demonstrate distinct strengths in finding visually similar images, global weight assignment might not be desirable when it comes to individual queries. For example, in particular object retrieval, Bag of Words (Bow) based methods encode local texture features such as SIFT and are effective in finding near duplicate objects. But these methods may fail when the query has a smooth surface [2]. On the contrary, global features such as GIST and HSV histogram present good capability in finding globally similar images. But when the query has rich and distinctive texture or has occlusions and truncation, the global features might fail. In another example, in the task of person recognition where one needs to find the photos containing the same person with a query, multiple visual cues could be leveraged, such as the face and clothes. However, due to variations in pose and camera viewpoint, faces are sometimes invisible, and sometimes a person may even change clothes, leading to unreliable or even harmful face/clothes features. Given a query, one should highlight those good features and suppress the bad ones, otherwise the retrieval accuracy may get even lower after fusion. In light of the above dilemma, it is natural to raise the question how to make an approximate estimation for the discriminative capability of features for a specific query. This problem is not trivial: some state-of-the-art fusion methods, as will be shown, suffer from the inclusion of black sheep features.

Another issue that should be paid attention to includes the amenability of the fusion method to database updating. It requires that the fusion algorithm be independent on the testing database, so that its effectiveness can be preserved in an updated database. Although offline calculations are necessary for effective fusion, one should be aware that an

- Z. Wang and S. Wang are with the Department of Electronic Engineering, Tsinghua University, Rohm Building 6-202, Beijing 100084, P.R. China. E-mail: wcd17@mails.tsinghua.edu.cn, wgsj@tsinghua.edu.cn.
- L. Zheng is with the Research School of Engineering, Australian National University. E-mail: liangzheng06@gmail.com

image database keeps growing, and it is desirable that the offline steps are not dependent on it. For this issue, some prior art requires expensive offline computations, and the resulting systems are rigid to database change.

To address the above challenges, this paper introduces a query-adaptive late fusion method for image retrieval. The proposed method has an unsupervised (hand-crafted) version and a supervised (learning) version, both based on a simple motivation shown in Fig. 1. We observe that since good features usually generate high scores for true matches and low scores for false matches, the sorted score curve is expected to have an elbow point. In other words, the curve is "L" shaped. For bad features, the scores of true matches cannot be distinguished from false matches, so the sorted score curve tends to be descending smoothly and steadily.

The query-adaptive strategy is designed based on the above observation. Using this idea, we introduce two versions of query-adaptive late fusion to address different retrieval tasks, *i.e.*, unsupervised and supervised. On the one hand, the unsupervised fusion scheme is proposed for scenarios like generic object retrieval. In this task, no prior knowledge on the topic of the query image is provided, since the nature of generic image search is unsupervised. In the proposed method, the score curves are firstly normalized by reference curves trained on irrelevant data, which are expected to approximate the tails of the initial score curve. Then, feature effectiveness is estimated as inversely proportional to the area under the normalized score curve (see Fig 2 for the pipeline). In the unsupervised fusion scheme, the offline operation is independent on the test database, making it well suited to dynamic systems where the database keeps growing. More importantly, our method identifies "good" and "bad" features on the fly, and the results are competitive to the state-of-the-arts on two particular object retrieval datasets.

On the other hand, for tasks such as person recognition and pedestrian retrieval, we introduce a supervised counterpart. Under this scenario, we are provided with informative labels which are beneficial for the system. Moreover, since the image content is fixed, the variance of score curve distribution is relatively small, making it easier to fit with a parametric model. Experimental results show that the query adaptive fusion module makes reasonable predictions of a feature's effectiveness. For instance, in person recognition, if the query is a man captured from the back view, our method will down-weight the "face" feature by assigning a low weight to it. Using the adaptive weight for complementary features, we produce comparable results against the state-of-the-art methods on the PIPA and Market-1501 datasets.

The remainder of this paper is organized as follows. First, we briefly review the related works in Section 2. Then, Section 3 introduces the component features to be fused in experiment. We describe the query-adaptive fusion method in Section 4. The experimental results are presented in Section 5 and conclusions are given in Section 6.

2 RELATED WORK

Image retrieval is a fundamental problem in computer vision. Among all the sub-tasks, particular object retrieval is a widely studied problem, aiming at searching in a

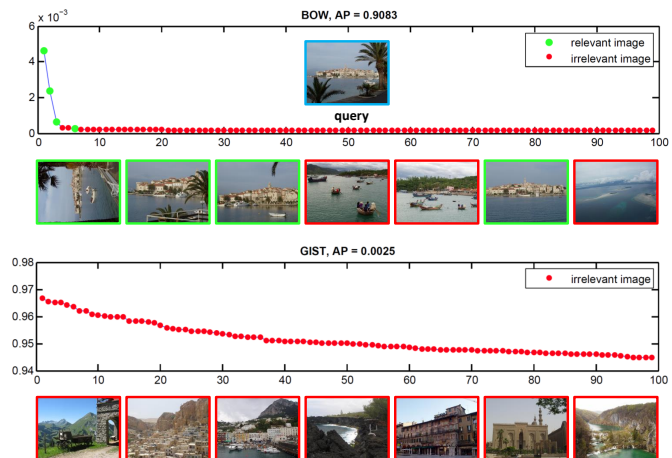


Fig. 1. Example of a multi-feature system. For a query (blue box) in the Holiday [12] dataset, the SIFT (upper) and GIST (bottom) features are employed to obtain two score lists respectively. There are four relevant images for this query, where SIFT produces good performance (AP = 90.83%), but GIST fails (AP = 0.25%). We plot the sorted scores for rank 1-99, and the corresponding 7 top-ranked images. True matches are marked in green, and false matches red. Note that the sorted score curve is L-shaped for SIFT, but descending smoothly and steadily for GIST.

database (gallery) for all the relevant targets to a specific query (probe) object. The target objects usually vary from common objects [24] to buildings [12], [27], [28]. Several descriptors present heterogeneous descriptive capability for images. Color histogram and GIST [26] encode the holistic images into a global feature so that images which have similar features look alike at a glance, but the content in the images may be irrelevant due to the neglect of local structures. The SIFT [22] descriptor delineates local structure in an image and shows robustness against variations of rotation, brightness, and scales, but tends to be helpless when imposters are a smooth surface [2]. In order to take full advantage of the strength of each feature, prior arts [38], [45], [46], [49] propose various fusion methods. Based on the BoW structure, local features such as color, can be combined with texture [34] or SIFT either by a Bag of Colors (BoC) [38] or the coupled Multi-index (c-MI) [49]. Both methods work on the indexing level, using complementary cues to filter out false positive SIFT matches. Zhang et al. [46] propose a co-indexing approach to expand the inverted index towards semantic consistency among indexed images. Furthermore, Rank Aggregation [14] fuses rank lists generated by different features by voting, which is straightforward but easily fails when rank lists have no overlaps. Another good practice consists in propagating the rank list along nodes in a graph [19], [36], [45]. In [45]. Through link analysis on a fused graph, local and global rank lists are merged with equal weight. In [36], a graph-based learning method is proposed to integrate multiple modalities for visual re-ranking. These methods, as mentioned, are flawed in either of the following two aspects. First, complementary features are assumably employed, so there is no fall back if an ineffective feature is integrated. Second, reranking methods such as [45], [46] heavily rely on the offline steps: all images in the database should be queried and the ranking results

are saved. This is potentially problematic if new images are constantly added to the database, and the offline works should be performed all over again.

In biometric systems, multimodal features provide heterogeneous information which can be fused, but the properties and calculation algorithms of such features are dramatically different, giving rise to the difficulties in feature level early fusion. As a consequence, to compensate for the limitations in the performance of individual features, late fusion receives extensive attention. Nandakumar et al. [23] model the distributions of genuine and impostor match scores as the finite Gaussian mixture model. Jain et al. [10] propose to transform the match scores to a common domain and the normalization schemes are data-dependent. The classifier output can also be combined using a supervised non-Bayesian method [33] which minimizes classification error under l_1 constraints. For each sample, these methods determine a fixed weight for a specific classifier and does not adapt to sample variations. In [11], user-specific weights are used, but it requires laborious collection of training samples over months.

Similar to biometric recognition / retrieval, person recognition [44] is also a multi-feature system where different visual cues are expected to be fused to draw on each other's strength. Person recognition can be connected to face recognition [7], [15] and person re-identification (retrieval) [7], [15] [29], [47]. Face recognition typically retrieves a target person with a near-frontal face image. Pedestrian retrieval seeks the target person with a holistic human body image in low resolution (where detailed regions like faces are often not distinguishable). In comparison, the person recognition task aims to recognize people in high resolution images such as photos in social media photo album. Despite the high image resolution so that visual information like faces and clothes can be exploited, these images present large variations in pose, clothing and camera viewpoint. Person recognition poses its unique challenge: 1) human faces may be invisible; 2) the target person wears different clothes from the query. Therefore, the face / clothes features are not always reliable or even harmful for recognition. In this area, previous works usually adopt a global weight strategy. That is, the weight of face and clothes features does not change *w.r.t* the query. For example, Oh et al. [25] fine-tune multiple AlexNets [17] with six visual parts and directly concatenate the features. Zhang et al. [44] and Kumar et al. [18] train pose-specific models and fuse the output similarity score either by directly summing or learning uniform weights for each model. Liu et al. [21] propose to learn more discriminative part features via Congenerous Cosine Loss and finally fuse similarity scores by weighted sum, in which the weights are regressed in the validation set and uniform for a particular feature. None of the aforementioned work considers assigning query adaptive weights to heterogeneous features. In fact, as to be shown later, being able to assign weights in a query-adaptive manner is essential to boost the retrieval performance and enhance the reliability of the systems.

3 HETEROGENEOUS FEATURES FOR VARIOUS TASKS

In this section, we provide a brief introduction to the to-be-fused heterogeneous features. A set of features can be categorized into two types: 1) features extracted by different descriptors, and 2) features extracted by different visual regions. Below, we will describe the heterogeneous features used in four important visual tasks.

3.1 Particular Object Retrieval

In particular object retrieval, features extracted by different descriptors are fused, namely BoW, HSV histogram, GIST, Random Projection and features from the convolutional neural network (CNN).

- **Bag-of-Words (BoW).** We adopt the baseline in [12], and the implementation setup in [49]. Hessian-Affine detector and SIFT descriptor are coupled in feature extraction. A 20k codebook is trained on Flickr60k dataset [12]. We use 128-bit Hamming signature with the Hamming threshold and weighting parameter set to 52 and 26, respectively. We also employ root-SIFT [3], average IDF [48], and the burstiness weighting [13]. Standard inverted index is leveraged, and the scores are l_2 -normalized.
- **HSV Histogram.** For each image, we compute an l_2 -normalized, 1,000-dim HSV histogram. The number of bins for H, S, V are 20, 10, 5, respectively.
- **GIST.** We calculate an l_2 -normalized, 512-dim GIST [26] descriptor. The images are resized to 256×256 . Four scales are used, and the number of orientations for each scale is (8, 8, 8, 8).
- **Features.** Recent convolutional neural network based features demonstrate promising performance in image retrieval, integrating both local and global descriptive capability [4], [35]. We adopt the state-of-the-art and publicly accessible model in [4] to extract an l_2 -normalized, 2048-dim convolutional feature.
- **Random Projection.** To illustrate the robustness of our method to bad features, we generate a random transform matrix $P \in \mathbb{R}^{d \times m}$ [39], where d is the target feature dimension (set to 1000 in our experiment), and m is the dimension of the input image (with all pixels concatenated by columns). Entries in P are sampled independently from a zero-mean normal distribution, and each row is l_2 -normalized to unit length. In effect, the resulting d -dim feature vector y is computed as $y = Px \in \mathbb{R}^d$, where x is the column-wise input image.

3.2 Person Recognition

In person recognition, we employ the features extracted by different regions. To be specific, four regions are used, *i.e.*, face, head, upper body and holistic body.

- **Face.** The head bounding boxes are given in PIPA [44] dataset. We employ a face detector [43] to detect the accurate locations of faces inside the head bounding boxes. If not detected, which means the face is usually profile or even does not appear, a

centric region in the head bounding box is extracted as the face. The faces are then aligned with five facial landmarks. Finally the aligned faces are fed into a 20-layer ResNet and we take the output 512-dim embedding as face features.

- **Head.** We cropped the heads according to the bounding boxes and then feed them into an Inception-v3 network. The output features are 2048-dim.
- **Upper body.** Given a head bounding box with up-left location (x, y) and size (w, h) , we estimate the upper body to be a box at $(x - 0.7w, y)$ with size $(2.4w, 3h)$, then the cropped image is fed into an Inception-v3 network and output the feature of upper body.
- **Holistic body.** We estimate the holistic body to be a box at $(x - 0.7w, y)$ with size $(2.4w, 5.5h)$, then the cropped image is fed into an Inception-v3 network and output the feature of holistic body.

3.3 Person Re-identification (Retrieval)

In person re-identification (retrieval), we adopt features extracted from body regions as well, which is consistent with recent state of the art [31], [37]. Body regions (parts) can be discovered either by unsupervised region proposals [31], [41] or from pose estimation results [37]. In this paper, we choose the Part-based Convolutional Baseline (PCB) proposed by Sun et al. [31] for its state-of-the-art performance and simplicity in implementation. PCB is a single-branch network which is able to produce multiple part features.

Using PCB [31] as our feature extractor, we reproduce it and set the number of features to 6 as recommended. In this paper, **the heterogeneous features refer to those extracted from the uniformly partitioned pedestrian regions from the top to the bottom.** The similarity scores produced by different features are used for further fusion.

For particular object retrieval (Section 3.1), person recognition (Section 3.2) and person re-identification (Section 3.3), the experimental datasets and the performance of each individual feature will be described in Section 5.

4 OUR APPROACH

4.1 Similarity Function

In literature, several strategies are commonly used to combine the scores of multiple features in order to obtain a global confidence measure [1], [16], e.g., the *sum*, *product*, *maximum*, *minimum* rules. Among the rules, the sum rule present the best capability in filtering out false positives, but suffers from variant scales of the input scores sensitively. On the other hand, previous works in biometric multi-modality fusion [1], [16] demonstrate that the product rule has very similar, if not superior, performance to the sum rule. The product rule also has another advantage: it adapts well to input data with various scales and does not depend heavily on a proper normalization of the data. In our work, we adopt the product rule in particular object retrieval, since the to-be-fused features have different algorithmic procedures and thus the scores may vary in their scales. But for person recognition / pedestrian retrieval we choose to merge score lists by the sum rule because the to-be-fused features are generated from different human parts by the

same algorithm, so the scales of the scores are basically the same.

Specifically, when K features are fused, given query q and a database image d , the similarity score of d to q w.r.t feature $\mathcal{F}^{(i)}$, $i = 1, \dots, K$ is denoted as $s_{d,q}^{(i)}$. Let $w_q^{(i)}$, $i = 1, \dots, K$ encode the weight of feature $\mathcal{F}^{(i)}$ for query q , in which $\sum_{i=1}^K w_q^{(i)} = 1$ is satisfied. Then, under sum and product rule, the similarity between q and d is respectively defined as,

$$s_s(q, d) = \sum_{i=1}^K w_q^{(i)} s_{d,q}^{(i)}, \text{ where } \sum_{i=1}^K w_q^{(i)} = 1, \quad (1)$$

$$s_p(q, d) = \prod_{i=1}^K (s_{d,q}^{(i)})^{w_q^{(i)}}, \text{ where } \sum_{i=1}^K w_q^{(i)} = 1. \quad (2)$$

Note that Eq. 2 can be transformed into a sum form by $\log(\cdot)$ operator.

4.2 Best and Worst Features

Let us first discuss the extreme cases, i.e., the most desirable and the most undesirable features for a given query q . We assume for simplicity that in an image collection with N images 1) there is only one relevant image j^* to q and 2) the image scores are normalized so that the scores range in $[0, 1]$. Intuitively, the most desirable feature satisfies the following criteria,

$$s_{j,q}^{(best)} = \begin{cases} 1, & j = j^* \\ 0, & otherwise \end{cases}, j = 1, 2, \dots, N, \quad (3)$$

where $s_{j,q}^{(best)}$ is the score of image j to query q w.r.t the best feature. In this case, only the relevant image j^* receives a score of 1, and all the irrelevant images 0. To the opposite, the worst feature for query q identifies itself as assigning a score of 0 to image j^* but 1 to the others, i.e.,

$$s_{j,q}^{(worst)} = \begin{cases} 0, & j = j^* \\ 1, & otherwise \end{cases}, j = 1, 2, \dots, N. \quad (4)$$

The score curves defined by Eq. 3 and Eq. 4, once sorted, exhibit a perfect L and a horizontal line, respectively. Ideally, in Eq. 1 and Eq. 2, weight of the best feature should be $w_q^{(best)} = 1$ and that of the worst feature should be $w_q^{(worst)} = 0$. **We find that the weight is negatively related to the area under the sorted score curve.**

4.3 Unsupervised Query Adaptive Fusion (QAF)

We first introduce the unsupervised version of query adaptive fusion. In many applications such as particular object retrieval, the image content can be very diverse, making it difficult to apply large-scale supervised learning on each semantic categories. Also, when the features are very different in their computation algorithms, the scales of scores vary a lot across different features. Therefore, we propose to design an *unsupervised* fusion scheme to avoid these problems. The proposed method is described below.

Reference Construction. In our method, a critical component is the reference curve, which is used to offset the tail of a testing score curve. In Fig.2(a), from the profiles of the three initial score curves, it is easy to tell that SIFT is

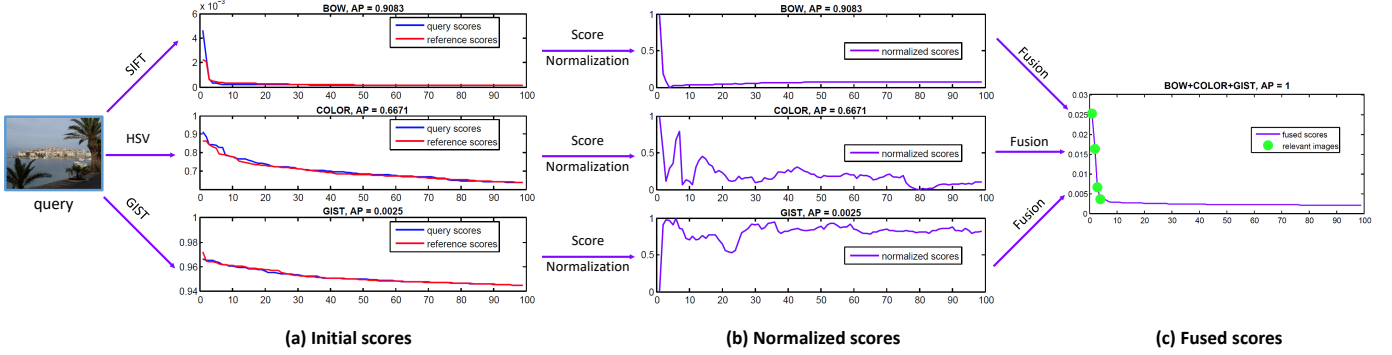


Fig. 2. Pipeline of the proposed unsupervised query adaptive fusion. Given a query image, three features (SIFT, HSV and GIST) are used to obtain initial rank lists. (a) The sorted initial scores are shown for rank 1-99 in blue curves, and the selected reference is depicted in red. (b) The score curves are eliminated by the reference, and the resulting scores are normalized by min-max normalization. (c) After calculating the feature importance through (b), we obtain the final score curve by Eq. 2. The three features obtain APs of 0.9083, 0.6671 and 0.0025 respectively, and the fusion result is AP = 1.0000. The calculated query-adaptive weights are 0.69, 0.30 and 0.01 for SIFT, HSV and GIST, respectively.

a good feature for this query. But the effectiveness of HSV and GIST is not so obvious: both curves have a relatively “high” tail, and scores of the top-ranked images are not remarkably higher than the tail. This is expected, because the color and GIST are global descriptors, and there would be more images that share a similar global appearance with the query. In other words, the underlying score distribution of a feature is not considered.

In order to alleviate the impact of “high” tails, this paper proposes to simulate the tail distribution of the initial score, by finding a reference score curve for each query. This reference score curve, if subtracted from the initial curve, would highlight the protrusion of the top-ranked scores, if any. In practice, we use independent datasets for reference collection. Specifically, for SIFT reference construction, we use the Flickr1M dataset released in [12]. It contains only the SIFT descriptors, which is compatible with SIFT descriptors used in the test datasets. For the other features, we crawled 1M high-resolution images using the names of 343 countries and regions across the world, called Flickr343Places dataset. Images in this dataset vary from scenes to objects and can be viewed as a good sampling of natural images.

In reference construction, we randomly select Q images as queries. Then, particular object retrieval is performed on Flickr343Places (for HSV, CNN, GIST, and random features) or the Flickr1M (for SIFT) dataset. All the resulting image scores are sorted. Together, we collect a codebook consisting of Q score lists for feature $\mathcal{F}^{(i)}$, denoted as $\mathcal{R}^{(i)} = \{r_h^{(i)}\}_{h=1}^Q$. Recall that the reference score lists are obtained on a dataset where all images are assumed to be irrelevant to each other. Therefore, the reference is able to represent the tail distribution of a score curve.

Another consideration is that the collected references should roughly be of the same length as the initial score curve, so that the score distribution would be similar. To this end, if the testing database contains N images, we should use roughly N irrelevant images for reference calculation. For large-scale datasets where N is large, both the initial score list and the references are down-sampled before the next step. In this manner efficiency is guaranteed.

Query-Adaptive Feature Weighting. After the reference codebooks are constructed in the aforementioned offline

method, during the online procedure, give query q , the only accessible information we have *w.r.t* feature $\mathcal{F}^{(i)}$ is the sorted score curve $s_q^{(i)}$. The profile of good feature should take on an “L” shape, while that of a bad feature a gradually descending curve (see Fig.1 and Fig.2).

From this observation, we propose to calculate the area under the image score curve, which is taken as the indicator to feature effectiveness. As indicated above, we seek to eliminate the high tail through the subtraction by a proper reference curve. Specifically, given an initial sorted score list $s_q^{(i)}$ obtained by feature $\mathcal{F}^{(i)}$, we aim to find in $\mathcal{R}^{(i)}$ a reference which best matches the tail of $s_q^{(i)}$. For this strategy, the simplest method consists in finding the code in codebook $\mathcal{R}^{(i)}$ which has the smallest Euclidean distance to $s_q^{(i)}$, *i.e.*,

$$r_q^{(i)*} = \arg \min_{r_h^{(i)} \in \mathcal{R}^{(i)}} \|s_q^{(i)}(u:v) - r_h^{(i)}(u:v)\|_2, \quad (5)$$

where $h = 1, 2, \dots, Q$, and u, v are parameters that restrict a curve segment on which the nearest neighbor is searched. Basically, it is required that v be relatively large to capture the tail distribution. Alternative to nearest neighbor search, the tail of a score curve can also be approximated by 1) k -nearest neighbor (k NN) search followed by an averaged sum, 2) sparse coding using $\mathcal{R}^{(i)}$ as the codebook. In Section 5.1 we will evaluate the sensitivity to parameter u, v, Q and also the three reference search method, *i.e.*, NN, k NN, and sparse coding.

In the next step, the reference is subtracted from the initial score curve of the query,

$$\hat{s}_q^{(i)} = s_q^{(i)} - r_q^{(i)*}. \quad (6)$$

Here, as shown in Fig.2(b), the reference closely approximates the profile of the tail distribution, so that scores of the top-ranked images can be highlighted in the resulting curve $\hat{s}_q^{(i)}$. Subsequently, $\hat{s}_q^{(i)}$ undergoes min-max normalization,

$$\bar{s}_q^{(i)} = \frac{\hat{s}_q^{(i)} - \min \hat{s}_q^{(i)}}{\max \hat{s}_q^{(i)} - \min \hat{s}_q^{(i)}}, \quad (7)$$

where $\bar{s}_q^{(i)}$ is the normalized score curve for feature effectiveness estimation. To illustrate the working mechanism

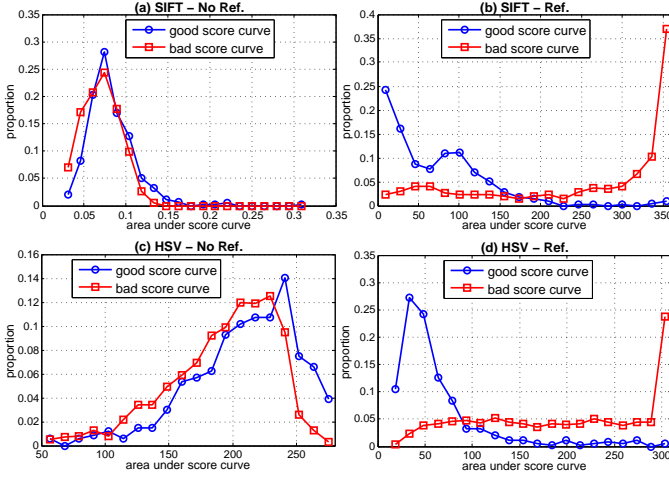


Fig. 3. Impact of reference subtraction. We calculate the proportion of good and bad score curves against the area under the score curve. Without reference, for (a) SIFT and (c) HSV features, good and bad curves cannot be distinguished. But when reference is subtracted, for (b) SIFT and (d) HSV features, good and bad curves are clearly separated.

of reference subtraction, for SIFT and HSV features, we have collected some good and bad score curves from Holidays and Flickr343Places datasets, respectively. Good score curves are those in which rank-1 image is a true match, and bad curves are assured by the irrelevance assumption in the Flickr343Places dataset. We calculate the proportion of good and bad score curves against the area under the score curve in Fig. 3. We find that after reference normalization, good queries tend to have a small area under the score curve, and vice versa. In this way, we can roughly tell the effectiveness of a feature after reference subtraction.

For a given query q with K features $\{\mathcal{F}^{(i)}\}_{i=1}^K$, we have K score lists $\{s_q^{(i)}\}_{i=1}^K$. After normalization to $\{\bar{s}_q^{(i)}\}_{i=1}^K$, the query-adaptive weight of feature $\mathcal{F}^{(i)}$ to q is determined as,

$$w_q^{(i)} = \frac{\frac{1}{A_i}}{\sum_{k=1}^K \frac{1}{A_k}} \quad (8)$$

where $A_i, i = 1, \dots, K$ represents the area under the i^{th} feature's score curve. We substitute Eq. 8 for Eq. 2 and obtain the desired query-adaptive similarity measurement.

Discussion. The proposed unsupervised fusion method is featured in two aspects. First, for a given query, we estimate a features effectiveness in a query-adaptive manner. While existing methods [45], [46] assign fixed weight to all features, our system is more robust to the impact of ineffective features. Second, by constructing a reference codebook offline, the estimation can be performed on-the-fly. Since our method does not require updating the reference codebook, and the nearest neighbor search is very fast, it can be well applied to large-scale and dynamic systems.

4.4 Supervised Query Adaptive Fusion (S-QAF)

In this section, we will introduce the supervised query adaptive fusion (S-QAF), which shares the similar spirit with its unsupervised counterpart (Section 4.3). Unlike particular object retrieval where the content of the to-be-searched target is not limited, sometimes in practice, we aim to search

a specific category of targets. Person recognition is one such task, in which the searched targets are all persons and we need to search for images with the same identity as the query in a database. The main challenges lie in the large variations in body poses, views, and consequently, severe deformations and even invisibility of body parts. On the one hand, in some photos, faces are commonly partially visible or even invisible. In such cases, the “face” feature would be unreliable, while it would be more reasonable to look at the “body” feature. On the other hand, if a person changes his / her clothes or hair-style, the “body” or the “head” features would be unreliable, while it would be more reasonable to look at the “face” feature. This motivates us to apply query adaptive fusion to human part features. In spite of the effectiveness and generalization of the aforementioned unsupervised query adaptive fusion (Section 4.3), we propose a supervised version for such content-specific retrieval tasks. The reason why we utilize supervised learning is two-fold. First, the informative labels are can be utilized, making it possible to learn to generate the optimal adaptive weights for each feature in an end-to-end manner. Second, the input content of the feature extractors is limited, so the distribution of the feature is limited. Consequently, the distribution of the similarity scores is also not as “diverse” as in particular object retrieval, making the patterns of “good” features and “bad” features embodied in the score curves more distinct. Below, we will describe the supervised version from two aspects, *i.e.*, the model and the optimization objective.

Model. For a specific query, the query adaptive fusion module takes as input multiple sorted score curves and outputs the corresponding weight for each features. For instance, in person recognition, we extract four part-based features from a person, *i.e.*, face, head, upper body and holistic body. For each feature, we compute the cosine similarity between the query and the whole database, yielding a similarity vector $s_{d,q}^{(i)}$. Once sorted, the similarity vector $s_{d,q}^{(i)}$ presents a descending curve, and we denote the sorted score curve as $s_q^{(i)}$. The sorted score curves can be regarded as 1-D signals, from whose magnitude and differentials we can infer its effectiveness for the query. We observe that the top m scores of $s_q^{(i)}$ contain most of the information, because the tail of the curve is close to a constant level. Therefore, the top m of the score curve, denoted as $s_q^{(i)}(1 : m)$, is cut off as the input of the model. Score curves of different features are stacked along an extra dimension, similar to the “channel” dimension in images, and we denote the stacked curves as $S_q^m, S_q^m = [s_q^{(1)}(1 : m), \dots, s_q^{(K)}(1 : m)]^T$. Given S_q^m as input, we train a small neural network $f(S_q^m; \theta)$ parameterized by θ . We utilize 1-D convolutional filters to process the input to better capture of the differentials of the signal. In person recognition experiment, we set the number of features K to 4, and set m to 100. The network structure and input / output size is presented in Fig.4. The output of $f(S_q^m; \theta)$ is a vector of size K which is summed up to 1. It is expected to approximate the optimal $w_q^{(i)}$.

Optimization Objective. A brute-force solution to generating query adaptive weights is to manually define or search the optimal weights for features of a specific query,

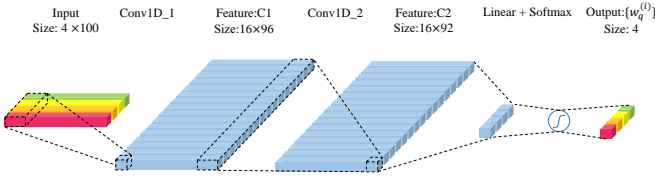


Fig. 4. The network structure used in the proposed S-QAF method for person recognition (number of heterogeneous features $K = 4$). For all the convolutional filters, kernel size is 5×1 , and stride is 1.

and use them as the supervision signals to train $f(S_q^m; \theta)$. However, it must not be optimal if we manually define the “ground truth” weights, since we could not quantify the importance of features accurately. Searching for optimal weights may be possible, but it needs a large amount of computation. Therefore, we propose to train $f(S_q^m; \theta)$ in an end-to-end manner.

The basic idea is directly optimizing the gap between the average score of true matches in the fused score curve and that of the false matches. Denoting the output of the network as $f(S_q^m; \theta) = (w_q^{(1)}, \dots, w_q^{(K)})$, we use them to replace the weights in Eq. 1 and obtain the unsorted fused score $s^f = \sum_{i=1}^K w_q^{(i)} s_{d,q}^{(i)}$. According to the labels of each candidate in training database and the label of the query, we categorize the scores in s^f into a true match set \mathcal{M}^+ and a false match set \mathcal{M}^- , i.e, for each s_i^f in s^f , $s_i^f \in \mathcal{M}^+$ if $y_i = y_q$, and $s_i^f \in \mathcal{M}^-$ if not $y_i = y_q$, where y_i and y_q are the labels of the i th database image and the query image, respectively. The optimization objective can be formulated as,

$$\mathcal{L}(s^f) = \max\left(\frac{1}{|\mathcal{M}^-|} \sum_{s_i^f \in \mathcal{M}^-} (d + s_i^f) - \frac{1}{|\mathcal{M}^+|} \sum_{s_i^f \in \mathcal{M}^+} s_i^f, 0\right), \quad (9)$$

where d is a margin term. We set $d = 1$ in all our experiment.

In practice, we also find it effective to mine *hard negative matches*. We sort scores of false matches in \mathcal{M}^- in descending order and pick $N_q^- = \alpha N_q^+$ false matches with the top scores as hard negative matches, where N_q^+ is the number of true matches for the specific query, and α is a balancing ratio. Instead of calculating the average score of all false matches as in Eq. 9, we only calculate the average score of hard negative matches. Mining hard negative matches makes the model converge to a better point, because the “easy” negatives dominate in number and would always yield low score once averaged. We set the ratio $\alpha = 2$ in our experiment.

5 EXPERIMENT

We first illustrate the tasks of particular object retrieval and person recognition in Fig.5. The goal of both tasks is to find the relevant targets to a query image in a gallery set, while the specific targets of each task are the particular object and particular person respectively. As shown in Fig.5, different visual cues (features) have different discriminative power, we show the merits of QAF and S-QAF by fusing these heterogeneous features.

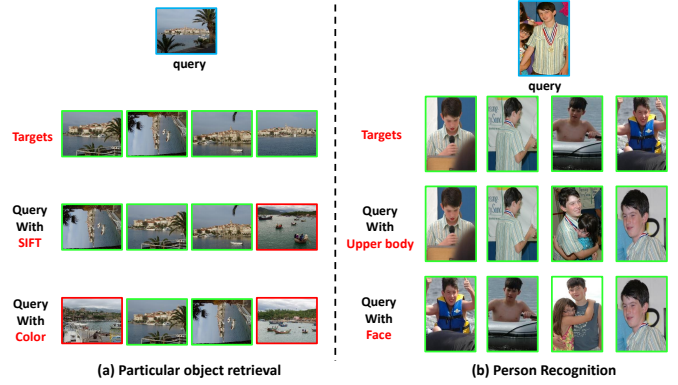


Fig. 5. Illustration on (a) *particular object retrieval* task and (b) *person recognition* task. We can observe that different visual cues have different discriminative ability.

5.1 Evaluation on Particular Object Retrieval

Datasets. We evaluate the proposed *unsupervised* fusion method on two particular object retrieval datasets, i.e., Ukbench [24] and Holidays [12]. The Ukbench dataset contains 10,200 images composed of 2,550 groups, each group has 4 images which are relevant to each other. Each image is taken as query in turn. We use N-S score as measurement, It counts the number of relevant images in the top-4 ranked images. The Holidays dataset is released with 1,491 personal holiday pictures. There are 500 queries in total. Mean Average Precision (mAP) is used as evaluation metric. It is the mean value of Average Precision (AP), which encodes the area under the precision-recall curve for each query.

Performance of individual features. Table 2 showcases the performance of individual features, i.e., SIFT encoded by BoW, Deep CNN, HSV, GIST, and random projections, on the two datasets. As we can observe, the up-to-date deep CNN based feature [4] presents satisfying performance on both datasets. Because the content of the images in Holidays are mainly scenery and landmarks, the high performance on Holidays greatly benefits from supervised training with a large-scale landmark dataset. On Ukbench, the fine-tuned CNN feature is reported to be less effective due to the inconsistency between training and testing data [5]. But the CNN feature still outperforms hand-crafted features. Given the individual features, we will demonstrate that the proposed fusion scheme is able to further boost the retrieval accuracy.

Parameter selection. Three parameters are involved in unsupervised QAF. We first evaluate the matching parameters u, v in Eq. 5, and the results are demonstrated in Fig. 6. We employ two types of CNN features here for comparison, one is the discriminatively learned deep retrieval model [4] (DR), and the other is an ImageNet pre-trained AlexNet (AN). The rest of the to-be-fused features are BoW, HSV, GIST and Random Projection. We observe that, as u and v vary, mAP is relatively stable for features that contains AN. For features that contains DR, $u = 1$ is the best choice. We speculate that it is due to the peaky distribution of the scores generated by DR. In other words, the score is either very close to 0 or very close to 1, so a small u is needed for highlighting the top scores. Performance of sparse coding is inferior, because the sparse control item has negative

TABLE 1

Results on two object retrieval benchmarks using different fusion methods. We compare our method with Rank Aggregation (RA) [14], Graph Fusion (Graph) [45], and global weight tuning (Global), respectively. BoW with Hamming Embedding [12] is used. Note that Graph fusion is sensitive to parameters, to be shown in Fig. 10.

Features					Holidays				Ukbench			
CNN	Bow	HSV	GIST	RAND	RA	Graph	Global	ours	RA	Graph	Global	ours
	✓		✓		52.00	76.39	81.54	80.88	2.429	3.674	3.610	3.590
	✓			✓	39.42	76.57	81.18	80.91	2.134	3.680	3.603	3.596
	✓		✓	✓	51.48	70.59	81.65	81.47	2.452	3.654	3.634	3.590
	✓	✓			83.79	71.98	84.18	84.47	3.538	3.808	3.745	3.755
✓			✓		52.34	81.61	93.32	92.96	2.385	3.851	3.835	3.833
✓			✓	✓	51.35	81.20	93.33	93.12	2.429	3.831	3.835	3.826
✓				✓	38.43	80.81	92.25	93.19	2.114	3.873	3.835	3.833
✓	✓				88.12	91.94	93.66	93.67	3.788	3.940	3.910	3.887
✓		✓			75.03	86.64	93.70	93.97	3.754	3.906	3.912	3.845
✓	✓	✓			91.36	92.61	94.17	94.08	3.870	3.945	3.920	3.902
✓	✓	✓	✓	✓	82.33	86.56	94.20	94.25	3.626	3.935	3.920	3.901

TABLE 2
Retrieval accuracy with individual features.

Datasets	CNN	BoW	HSV	GIST	RAND
Holidays, <i>mAP</i>	92.99	80.16	61.32	33.81	13.49
Ukbench, <i>N-S</i>	3.833	3.582	3.195	1.856	1.422

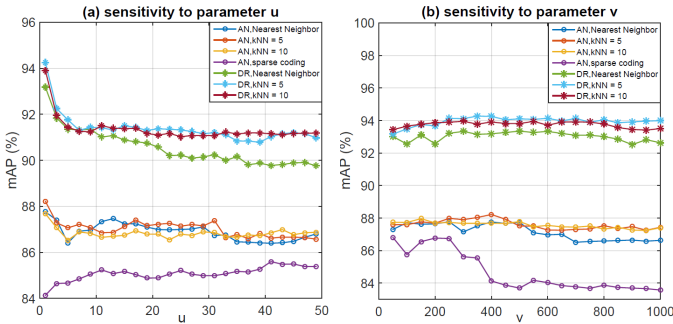


Fig. 6. Sensitivity to u and v on Holidays. Five features are fused, *i.e.*, CNN, BoW, HSV, GIST and Random Projection. *mAP* is plotted against the two parameters in Eq. 5. Four reference selection methods are compared, *i.e.*, nearest neighbor, k NN ($k = 5$ or 10), and sparse coding. We also explore different CNN features, *i.e.*, fine-tuned CNN feature trained with Deep Retrieval [5] (DR) and CNN feature extracted from an ImageNet pre-trained AlexNet (AN).

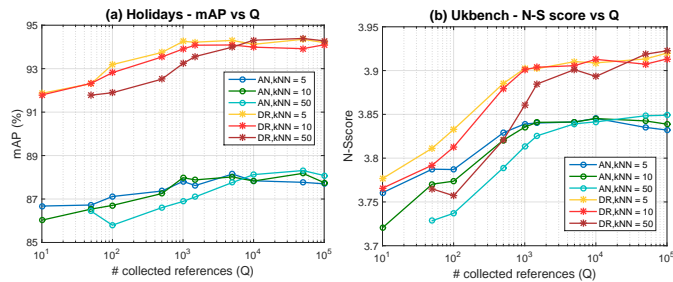


Fig. 7. Sensitivity to parameter Q on (a) Holidays and (b) Ukbench datasets. We test k NN = 5, 10, and 50. DR refers to Deep Retrieval as CNN feature extractor while AN refers ImageNet Pre-trained AlexNet as CNN feature extractor.

impact on the NN search item. Moreover, three NN-based methods perform similarly, and it seems that “ k NN = 5” is slightly superior. When using k NN, the averaged reference

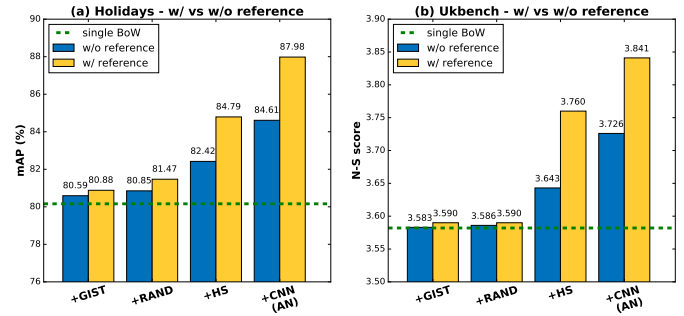


Fig. 8. The impact of reference. We compare our method with the case where reference is not used. Four feature combinations are presented, *i.e.*, “BoW + GIST”, “BoW + GIST + Random”, “BoW + GIST + Random + HS”, and “BoW + GIST + Random + HS + CNN”. The green dash line represents the BoW results, while blue and yellow bars show results by “without reference” and “with reference”, respectively. CNN features are extracted from an ImageNet pre-trained AlexNet (AN).

is more resistant to noise, but when k increases, more “bad” references are introduced especially under small Q . We set $u = 1$ and $v = 400$ in our experiment.

When evaluating parameter Q , *i.e.*, the size of the reference codebook, we present the results in Fig. 7. We find that the fusion accuracy increases steadily with Q . In fact, when Q is large, it is more likely to find among them a good approximation to the tail distribution. Nevertheless, computational complexity also increases with Q . Considering this, we choose $Q = 1000$ in our experiment as a trade-off between speed and accuracy.

Impact of the reference curve. To demonstrate the effectiveness of reference selection, we compare with the case in which no reference is used. In other words, the score curve directly undergoes min-max normalization, and the resulting area is employed for feature weight estimation. The results are shown in Fig.8. It is clear that, the usage of reference brings benefit for various feature combinations. On Holidays and Ukbench datasets, when all five features are fused, the usage of references brings improvement of +3.37% in *mAP*, and +0.115 in *N-S*, respectively.

Comparison with global parameter tuning. For each features, we assign to it a global weight $w^{(i)}$, $i = 1, \dots, K$ and search the optimal combination. When fusing five fea-

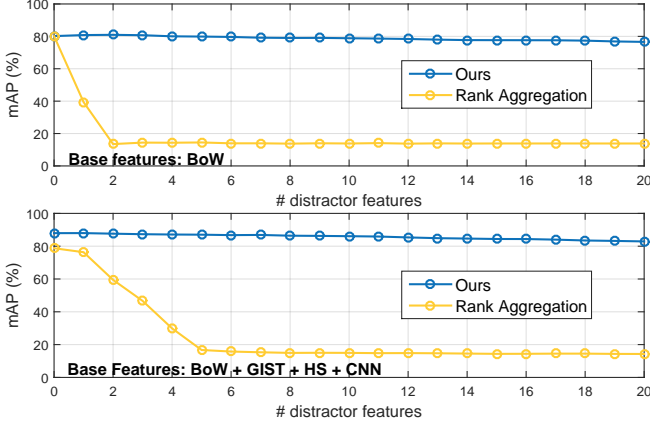


Fig. 9. Impact of bad features on Holidays dataset. We plot mAP against a increasing number of random features. Top: random features are fused with BoW. Bottom: BoW + GIST + HS + CNN (pre-trained AlexNet) is used as baseline. We compare with Rank Aggregation [14].

tures, we use a step of 0.1 for manual tuning. The results are shown in Table 1 (Global). We observe that our results are comparable, and sometimes even superior to the results of global tuning on the Holidays dataset. On Ukbench QAF (ours) also performs comparable to global tuning *without* tuning parameters. It demonstrates the effectiveness of our method.

Comparing with global parameter tuning, our method is advantageous in two aspects. First, for global tuning, the parameters should be tuned for different datasets. But our method automatically determines the weights, making it more generalizable to different datasets. Second, our method is very efficient in computing the query-adaptive weights, but global feature tuning needs to search over a large parameter space, and this is very time consuming.

Robustness to many “bad” features. When a large number of bad features are present, it is desirable that fusion result not be influenced too much. In our experiment, 20 random projection matrices are generated, so that we are provided with 20 random projection features.

We evaluate this property on the Holidays dataset in Fig. 9. We compare our method with Rank Aggregation (RA). In RA, we compute the median rank of each candidate image over all rank lists obtained by different features. We can see that when the number of random features increases, mAP of our method drops very slowly, but that of RA decreases dramatically. When as many as 20 “bad” features are used, mAP of our method drops from 80.16% to 76.58%, and from 87.98% to 82.91% for the two base-feature settings, respectively. In comparison, RA yields an mAP of 13.85% and 14.29%, respectively. Therefore, our method is very robust to “bad” features.

Comparison with other fusion schemes. In order to further verify the strength of our method, results of two fusion schemes, *i.e.*, Rank Aggregation [14] and Graph Fusion [45] are present in Table 1 and Fig. 10.

On both datasets, Rank Aggregation yields inferior performance to Graph Fusion and our method. This is mainly because rank aggregation requires voting from multiple rank results, so that when features are complementary to

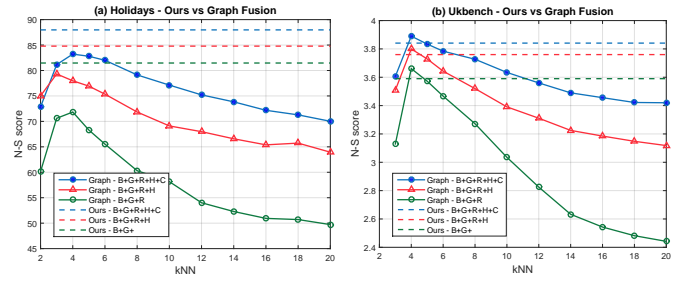


Fig. 10. Comparison with graph fusion. On (a) Holidays and (b) Ukbench datasets, three feature combinations are tested. Abbreviations B, G, R, H, and C represent BoW, GIST, Random, HSV, and CNN, respectively. CNN features are extracted by Deep Retrieval model [4]. Dashed lines are the results of our method. kNN refers to the key parameter in graph fusion.

each other, the intersection of the top-ranked candidates predicted by different features tends to be small. We can observe from Table 2 that when we combine CNN features with BoW and HSV features Rank Aggregation produces good results, because these features generate similar top candidates. For comparison, the performance drops dramatically when complementary features (GIST, Rand) are fused.

For graph fusion, we use the code released by [45]. Except for the k NN value (different from the k in our method), we use the default parameters. Results in Fig. 9 indicate that graph fusion is sensitive to parameter k NN, which, in order to obtain fine accuracy, should be consistent with the average number of true matches in the dataset. For comparison convenience, we plot the corresponding results of our method as the dashed lines.

On Holidays dataset, for each feature combination, our method outperforms Graph Fusion. On Ukbench, our result is lower than graph fusion only when k NN = 4, which is the ideal parameter setting on Ukbench, since the number of relevant targets is a constant, *i.e.*, 4, for every query. Nevertheless, when k NN is set to other values, the performance of graph fusion drops. Moreover, when bad features, such as GIST and Random are used, graph fusion does not have a fall back mechanism (in fact, it treats all the features as equally important). Considering that our method is robust to parameters (see Fig. 6 and Fig. 7), we speculate that our method yields more stable and accurate performance than graph fusion.

Complexity and Scalability. The proposed method can be broken down into two phases, *i.e.*, offline reference codebook generation and online query adaptive weight estimation. For the offline procedure, the complexity is $O(Q|\mathcal{I}|)$ where Q is the codebook size and \mathcal{I} is the irrelevant dataset for reference construction. Note that for a specific feature, we only need to construct the reference codebook once for all, so it does not matter if $|\mathcal{I}|$ is slightly large.

In experiment, we perform a large-scale experiment by combining MirFlickr1M dataset [9] with Holidays dataset to test the scalability of the system. As noted in Section 4.3, we down-sample the initial score lists and references to a length of 1000. Moreover, dimension of all four global features are reduced to 128-D by PCA. Our experiments are performed on a server with 3.46 GHz CPU and 128

TABLE 3

Average query time (s) of different steps on Holidays + 1M, feature extraction and quantization time excluded.

Stage	BoW	Glob. Feat.	Ref. Selection
Avg. Time (s)	1.95	0.96	0.01

GB memory. CNN features are extracted with a GTX 780 Ti GPU. The average query time and the breakdown are shown in Table 3. Our method adds little extra time in inference selection. Moreover, the storage of the reference codebook costs only 7.63MB extra memory. Therefore, our method is efficient in terms of memory and time cost. As comparison, graph fusion also adds neglectable time cost in graph analysis. However, it needs to compute pairwise distances of the union set of query and database images, which is $O((|Q| + |D|)^2)$ in complexity, where Q and D are the query set and database set respectively. When the database grows larger, the time cost increases dramatically. There is no such procedure in our method, so we only need to compute pair-wise distance between query and database which is only $O(|Q||D|)$.

5.2 Results on Person Recognition

Dataset and Evaluation Metric. We use the People in Photo Album (PIPA) dataset [44] for both training and evaluation. To our knowledge, the PIPA dataset is the first dataset collected for unconstrained person recognition. It consists of over 60,000 instances of 2,000 individuals collected from public Flickr photo albums. For each instance, a head bounding box is provided, regardless if the instance is in frontal view or in back view. For those in back view, annotators infer their identity by the clothes, the surroundings, and also the relationship with other identities, which guarantees the accuracy of the annotations. PIPA is challenging when using single visual cues due to the occlusion with other people, viewpoint, pose and variations in clothes. For instance, if we only pick faces as the retrieval cue, we would see that only 52% of the people have high resolution frontal faces suitable for recognition. Clothes are also a good appearance feature, but difficulties arise when different persons wear similar clothes (which is common in occasions like festivals or celebrations), or the same person appears in multiple albums wearing different clothes. All of the above difficulties make it very suitable to apply query adaptive fusion to person recognition.

The original test setting of PIPA in [44] considers person recognition as a classification task. In [44], a feature extractor is first trained on the training set, and then a classifier is trained on a subset of the testing set that contains all the identities of the testing set. This setting actually might deviate from practice, because it is impractical to train a new classifier every time a new identity is introduced during testing.

In this paper, we formulate person recognition as an open-set retrieval problem, where we use the top-1 accuracy as the evaluation metric. The top-1 accuracy is comparable to the recognition accuracy in the original close-set classification setting, since it can be regarded as the recognition accuracy of a nearest neighbor classifier. The open-set set-

TABLE 4

Top-1 accuracy of individual features on the PIPA dataset.

Feature	Original	Album	Time	Day
Face	65.08	63.49	61.04	61.22
Head	76.07	66.97	56.73	35.60
Upper Body	75.04	64.14	51.68	22.80
Body	68.11	57.01	43.16	16.93

ting is closer to practice because it does not need retrain classifiers when new testing persons are added.

In our protocol, the testing set is split into a query set and a gallery set. Following the setup in [25], we split the test set in four different ways, namely *original*, *album*, *time*, and *day*. The *original* setup is the easiest one, in which a query instance may have very similar appearance with its true matches in the gallery. The other three are more challenging. For example, the *day* setup enforces the query instances has appearance changes compared to the true matches, while the *time* setup emphasizes the temporal distance between query set and the gallery set. We test all the four setups. For each setup, we switch the query set and gallery set, so that we can have two testing results. The two results are averaged to obtain the final performance.

Implementation Details. According to Section 3.2, for each of the four body parts, namely face, head, upper body and holistic body, we separately train a CNN feature extractor. The face feature extractor is a 20-layer ResNet [6] trained with CASIA-WebFace dataset [42] and the A-Softmax loss [20]. All faces are detected by MTCNN [43] and aligned with five facial landmarks. We use the Inception-v3 [32] architecture for the other three feature extractors, and train them on the PIPA training set with the softmax loss. Hyperparameters for training face feature extractors are the same as in [20]. For all the extractors, we use SGD as the optimizer with learning rate 0.1, and decay by 0.1 at the 30th, the 45th and the 53rd epoch. The total number of epochs is set to 60, and the batch size is set to 128.

Performance of Individual Features. Table 4 showcases the performance of individual features in each setup. In the *original* setup, the head feature and upper body feature present good retrieval accuracy. This is expected, because the head and the upper clothes are two primary cues to search the same person. Theoretically, the holistic body should be more informative than the upper body, but in practice it suffers from misalignment, for example, if a person is sitting or lying, the holistic body bounding box would be inaccurate. Another observation is that the face feature has stable performance when the testing setup changes. In the *Day* setup, the face feature remains an accuracy of 61.22%, while performance of other features drops dramatically, especially the upper body and the holistic body features. This is because in the *Day* setup identities wear different clothes between the query set and the gallery set, so that the face feature and head feature are more reliable.

Unsupervised v.s. Supervised Query Adaptive Fusion.

In this section, we compare the proposed unsupervised query adaptive fusion scheme (QAF) with the supervised query adaptive fusion scheme (S-QAF). For QAF, we set $kNN = 5$, $u = 10$, $v = 400$, and $Q = 1000$. The reference

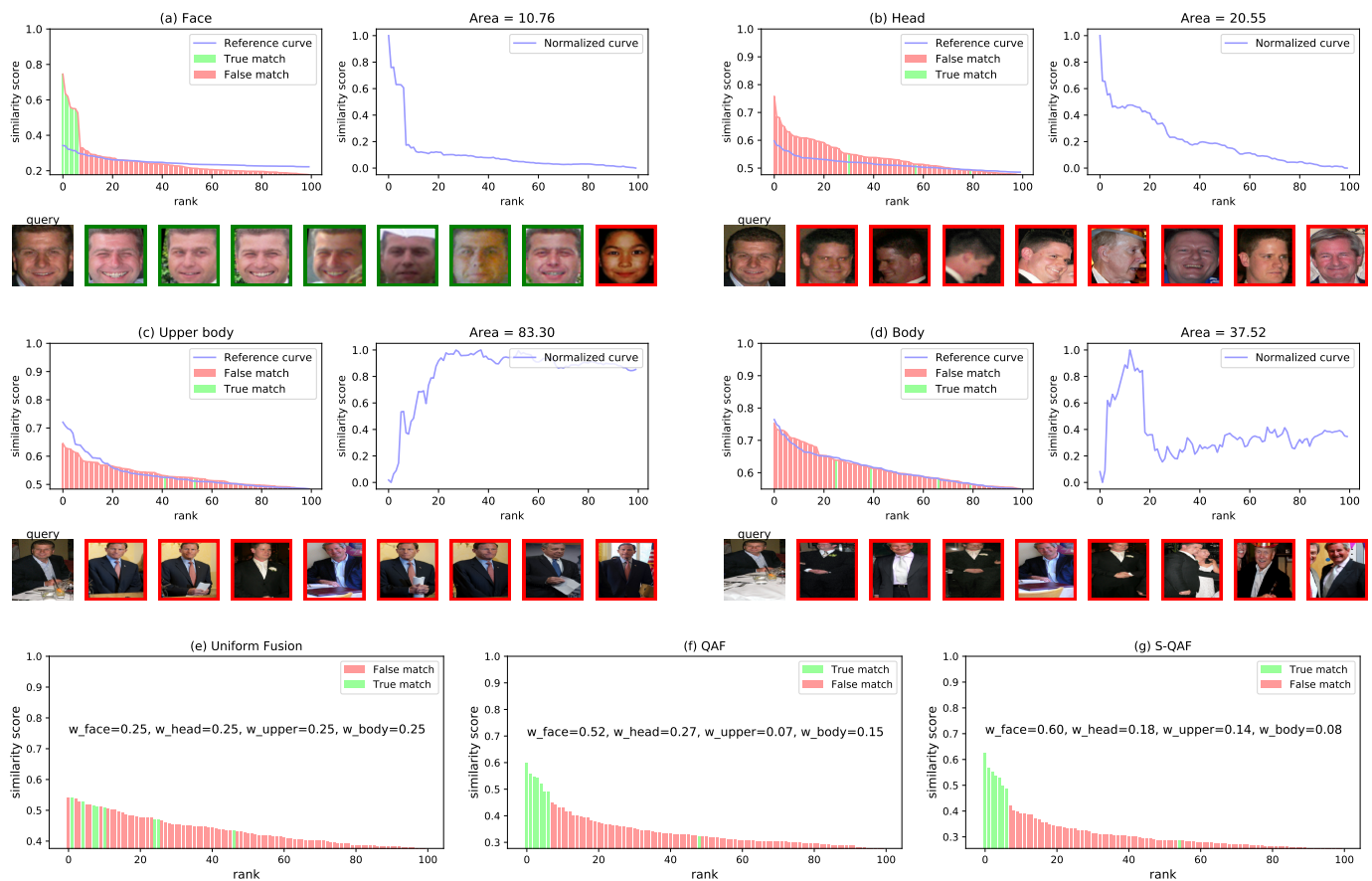


Fig. 11. Illustration of query adaptive fusion for person recognition. (a)-(d) present the score curves of face, head, upper body and holistic body features, the reference curve and normalized curve (for unsupervised query adaptive fusion), and also the top 8 candidate of the query for each feature. (e) presents the fusion result of uniform fusion, *i.e.*, assigning all features with the same importance. (f) and (g) shows the fusion results of the unsupervised query adaptive fusion (QAF) and the supervised query adaptive fusion (S-QAF), respectively. For this query, we observe that the face feature is the most important. Both QAF and S-QAF succeed in estimating the feature importance, while S-QAF is slightly superior since it assigns a larger weight to the face feature.

TABLE 5

Comparison with state-of-the-art results and other fusion schemes on PIPA.

Method	Original	Album	Time	Day
PIPER [44]	83.05	-	-	-
naeil [25]	86.78	78.72	69.29	46.61
Pose-aware [18]	89.05	83.27	74.84	56.73
COCO [21]	92.78	83.53	77.68	61.73
RANet [8]	89.73	85.33	80.42	67.16
<i>Global^{original}</i>	88.52	83.52	77.08	62.61
<i>Global^{album}</i>	87.74	83.68	77.91	67.60
<i>Global^{time}</i>	87.74	83.68	77.91	67.60
<i>Global^{day}</i>	85.59	82.34	77.09	68.85
Uniform	88.26	83.40	77.13	64.60
QAF	88.01	84.15	78.33	66.41
S-QAF	89.79	85.21	79.45	68.20

codebook is constructed with the PIPA training set. In the construction of each reference codebook, we first select one image of an identity as the query and use the images of other identities as database images to make sure there is no true match. For S-QAF, we train the S-QAF module with the PIPA validation set. Qualitative and quantitative comparisons

are present in Fig. 11 and Table 5 respectively.

Figure 11 shows a typical query instance in the *Day* setup: the database instances of the same identity wear different clothes *w.r.t* the query. In this case, the upper body and holistic body features are unreliable, while the face feature is discriminative. As shown in Fig. 11 (f) and (g), both QAF and S-QAF succeed in estimating the importance of the features. Moreover, S-QAF seems superior because it assigns a higher weight to the face feature. Table 5 compares QAF and S-QAF with the Uniform Fusion baseline in terms of retrieval accuracy. In the Uniform Fusion baseline, all the features are fused with the same fixed weight. Both QAF and S-QAF outperforms the baseline, indicating that the fusion schemes are effective. It is expected that S-QAF performs better than QAF, because the weights are learned end-to-end with a loss function which enlarges the gap between true matches and false matches.

Comparison with global fusion. In order to validate the effectiveness of QAF and S-QAF, we perform grid search to seek optimal global weights for each testing setups. By “global”, we assign a constant weight to a component feature, *i.e.*, not “query adaptive”. The step of the grid search is set to 0.1. The optimal results are demonstrated in the sec-

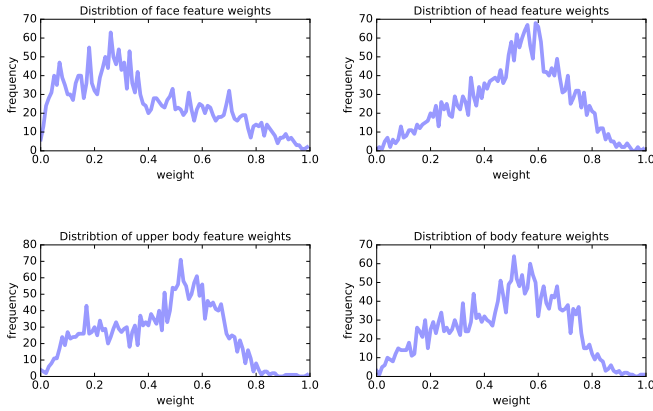


Fig. 12. Distribution of the feature weights of face, head, upper body, and holistic body generated by S-QAF under the PIPA *Day* setup.

ond part in Table 5. As expected, the optimal global weights for different testing setups are different. For example, the optimal weights are (0.2, 0.4, 0.2, 0.2) and (0.4, 0.3, 0.2, 0.1) for the *Original* and the *Day* setups, respectively. QAF exceeds the global fusion in two test setups (*Album* and *Time*), and S-QAF exceeds global fusion in three setups (*Original*, *Album* and *Time*). For those setups where QAF and S-QAF do not outperform the global fusion, the results are also competitive. The main benefit of QAF and S-QAF is their robustness to the change of test set. In other word, QAF and S-QAF performs well when the appearance change between query and gallery is large (the *Day* setup) and when the appearance change is small (the *Original* setup). In fact, if we assign global weighs to the heterogeneous features, we cannot find a single set of optimal weights that suits all test setups. It means we need to search for the weights for each datasets, which is very time-consuming. We also visualize the distribution of weights generated by S-QAF on PIPA *Day* test split. The results are shown in Fig. 12. The feature Weights are distributed scatteredly in the histogram. This indicates that the feature weights are determined in a query-adaptive manner and that the weights differ from query to query.

Comparison with state of the art. Comparison with the state-of-the-art results on PIPA are showcased in the Table 5. In some of the compared methods, auxiliary information is utilized to improve retrieval accuracy. For example, in [44] and [18], the human pose information is integrated. In [25] and [8], the scene information or the relationship among persons are analyzed. Liu et al. [21] use the most similar setting to us, *i.e.*, only the human appearance is used, and our performance is comparable with [21]. Comparing with these methods, we observe from Table 5 that the reported accuracy is very competitive.

Complexity and scalability. Tested on a server with 3.46 GHz CPU, 128 GB memory and a Titan Xp GPU, the average time cost for feature extraction for one query is 23.5 ms, 1.6 ms and 0.6 ms respectively. On top of the time for feature extraction, QAF and S-QAF add very little extra time cost in the fusion process. As for the memory cost, the codebook size of QAF is 8.46 MB, while the size of S-QAF model is

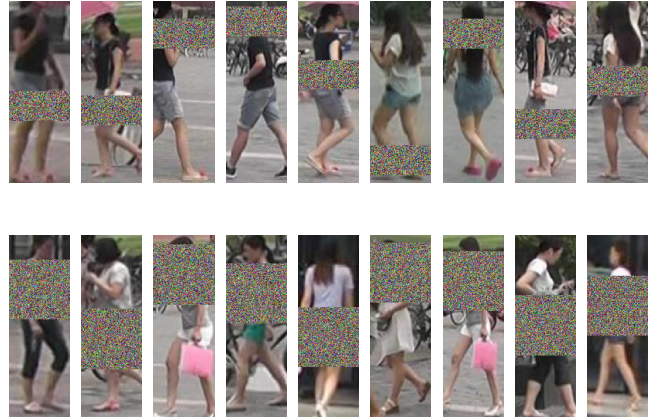


Fig. 13. Illustration of images under occlusion levels of $1/6$ (first row) and $1/3$ (second row). The definition of occlusion levels can be viewed in Section 5.3.

TABLE 6

Retrieval accuracy v.s occlusion level. Rank-1 accuracy and mAP are reported on the Market-1501 dataset. Two methods are compared, *i.e.*, feature concatenation (Concat.) and score-level averaging (Avg.).

		mehthod		
		Concat.	Avg.	S-QAF
No Occ.	mAP	75.4	75.2	73.5
	Rank-1	91.9	91.8	91.0
$1/6$ Occ.	mAP	28.3	26.5	32.8
	Rank-1	72.3	70.9	73.5
$1/3$ Occ.	mAP	12.2	11.3	15.4
	Rank-1	54.7	53.1	56.4

only 72.8 KB. Moreover, the computation cost of QAF and S-QAF does not increase with the size of the database, so both methods have good scalability.

5.3 Results on Pedestrian Retrieval

Dataset and Evaluation Metric. To further investigate the application scope of the proposed query adaptive fusion, we perform pedestrian re-identification (retrieval) experiment on the Market-1501 dataset [47]. It is one of the most widely used datasets in pedestrian retrieval, which consists of 19,732 gallery images and 12,936 training images from 1,501 identities. We use mAP and top-1 accuracy of the Cumulative Matching Characteristics (CMC) curve as evaluation metrics.

Occluded Pedestrian Retrieval. As it is designed to be, query adaptive fusion has the ability to estimate the importance of features. To validate this point, we perform experiment on occluded pedestrian retrieval, so that the part features have different discriminative ability. In order to simulate occlusion, we add a rectangle mask generated by Gaussian noise. Two occlusion levels are used, *i.e.*, $1/6$ and $1/3$, which denote the ratio of size of the mask to the size of the image. Note that the mask is located randomly. Examples are shown in Fig. 13. We use the part-based convolutional baseline (PCB) [31] as the pedestrian descriptor, which outputs six part-based features for a pedestrian image. The features are fused by three different methods, *i.e.*, directly concatenating at feature level, averaging at score level, and fusion with S-QAF at score level. We then observe

how the performance of different fusion methods vary *w.r.t* different occlusion levels.

The comparison results are shown in Table 5.3. Several conclusions can be made. First, when we add occlusion to the testing images, the performance drops dramatically. This is expected due to the information lost. Second, when occlusion is applied, S-QAF outperforms the two baselines, *i.e.*, feature concatenation and score-level averaging, indicating its ability to select and use the informative features. Third, when testing with original samples without occlusion, S-QAF is slightly inferior to the baselines. We examine the score curves and find that, in this case, all the component features tend to generate “good curve” (in which true matches are ranked at top). So the S-QAF module might generate less accurate estimation of feature importance. From this observation we speculate that, the proposed query adaptive fusion scheme would work at its prime if the to-be-fused features are not all “good” features. In such case the fusion scheme can assign reasonable weights to different features. This is also supported by the results in Section 5.2, where S-QAF is good at filtering out features of absence faces.

Discussion. Considering all the aforementioned experimental results, we find that query adaptive fusion works better if the following two conditions are satisfied. First, the features are complementary to each other. For a specific query, it is best if there exist both good features and bad features. If the features are all good or all bad, the importance estimation will be less accurate. Second, the feature has some decent discriminative ability, so it can generate a gap between the true matches and false matches. The gap is utilized for feature importance estimation.

6 CONCLUSION

In this article, we present query adaptive fusion for visual retrieval tasks. Our method leverages the ranking score curves to estimate the importance of heterogeneous features, and then fuses them. Specifically, for unsupervised tasks such as particular image retrieval, we propose an unsupervised fusion scheme (QAF); for supervised tasks such as person recognition, we proposed a supervised method (S-QAF). Both methods are able to estimate the feature effectiveness for a given query. In this way, “good” features are up-weighted and “bad” features are down-weighted. In our experiment, we show the proposed method is robust to parameter changes, is superior to several other fusion methods, and is robust when many “bad” features are present in the system. In the two tasks, *i.e.*, particular object retrieval and person recognition, we demonstrate that QAF and S-QAF are able to produce very competitive accuracy compared with the state-of-the-art methods. The applicable scope and the limitation of the proposed method is also investigated in an occluded pedestrian retrieval experiment.

REFERENCES

- [1] F. M. Alkoot and J. Kittler, “Experimental evaluation of expert fusion strategies,” *Pattern Recognition Letters*, vol. 20, no. 11-13, pp. 1361–1369, 1999.
- [2] R. Arandjelović and A. Zisserman, “Smooth object retrieval using a bag of boundaries,” in *Computer Vision (ICCV), 2011 IEEE International Conference on*. IEEE, 2011, pp. 375–382.
- [3] R. Arandjelovic and A. Zisserman, “Three things everyone should know to improve object retrieval,” in *CVPR*, 2012, pp. 2911–2918.
- [4] A. Gordo, J. Almazán, J. Revaud, and D. Larlus, “Deep image retrieval: Learning global representations for image search,” in *ECCV*, 2016, pp. 241–257.
- [5] —, “End-to-end learning of deep visual representations for image retrieval,” *International Journal of Computer Vision*, vol. 124, no. 2, pp. 237–254, 2017.
- [6] K. He, X. Zhang, S. Ren, and J. Sun, “Deep residual learning for image recognition,” in *CVPR*, 2016, pp. 770–778.
- [7] G. B. Huang, M. Ramesh, T. Berg, and E. Learned-Miller, “Labeled faces in the wild: A database for studying face recognition in unconstrained environments,” University of Massachusetts, Amherst, Tech. Rep. 07-49, October 2007.
- [8] Q. Huang, Y. Xiong, and D. Lin, “Unifying identification and context learning for person recognition,” in *CVPR*, 2018.
- [9] M. J. Huiskes, B. Thomee, and M. S. Lew, “New trends and ideas in visual concept detection: the MIR flickr retrieval evaluation initiative,” in *Proceedings of the 11th ACM SIGMM International Conference on Multimedia Information Retrieval, MIR 2010, Philadelphia, Pennsylvania, USA, March 29-31, 2010*, 2010, pp. 527–536.
- [10] A. K. Jain, K. Nandakumar, and A. Ross, “Score normalization in multimodal biometric systems,” *Pattern Recognition*, vol. 38, no. 12, pp. 2270–2285, 2005.
- [11] A. K. Jain and A. A. Ross, “Learning user-specific parameters in a multibiometric system,” in *ICIP*, 2002, pp. 57–60.
- [12] H. Jegou, M. Douze, and C. Schmid, “Hamming embedding and weak geometric consistency for large scale image search,” in *ECCV*, 2008, pp. 304–317.
- [13] —, “On the burstiness of visual elements,” in *CVPR*, 2009, pp. 1169–1176.
- [14] H. Jegou, C. Schmid, H. Harzallah, and J. J. Verbeek, “Accurate image search using the contextual dissimilarity measure,” *IEEE Trans. Pattern Anal. Mach. Intell.*, vol. 32, no. 1, pp. 2–11, 2010.
- [15] I. Kemelmacher-Shlizerman, S. M. Seitz, D. Miller, and E. Brossard, “The megaface benchmark: 1 million faces for recognition at scale,” in *CVPR*, 2016, pp. 4873–4882.
- [16] J. Kittler, M. Hatef, R. P. W. Duin, and J. Matas, “On combining classifiers,” *IEEE Trans. Pattern Anal. Mach. Intell.*, vol. 20, no. 3, pp. 226–239, 1998.
- [17] A. Krizhevsky, I. Sutskever, and G. E. Hinton, “Imagenet classification with deep convolutional neural networks,” in *NIPS*, 2012, pp. 1106–1114.
- [18] V. Kumar, A. M. Namboodiri, M. Paluri, and C. V. Jawahar, “Pose-aware person recognition,” in *CVPR*, 2017, pp. 6797–6806.
- [19] W. Liu, Y. Jiang, J. Luo, and S. Chang, “Noise resistant graph ranking for improved web image search,” in *CVPR*, 2011, pp. 849–856.
- [20] W. Liu, Y. Wen, Z. Yu, M. Li, B. Raj, and L. Song, “Sphereface: Deep hypersphere embedding for face recognition,” in *CVPR*, 2017, pp. 6738–6746.
- [21] Y. Liu, H. Li, and X. Wang, “Learning deep features via congeneric cosine loss for person recognition,” *CoRR*, vol. abs/1702.06890, 2017. [Online]. Available: <http://arxiv.org/abs/1702.06890>
- [22] D. G. Lowe, “Object recognition from local scale-invariant features,” in *ICCV*, 1999, pp. 1150–1157.
- [23] K. Nandakumar, Y. Chen, S. C. Dass, and A. K. Jain, “Likelihood ratio-based biometric score fusion,” *IEEE Trans. Pattern Anal. Mach. Intell.*, vol. 30, no. 2, pp. 342–347.
- [24] D. Nistér and H. Stewénius, “Scalable recognition with a vocabulary tree,” in *CVPR*, 2006, pp. 2161–2168.
- [25] S. J. Oh, R. Benenson, M. Fritz, and B. Schiele, “Person recognition in personal photo collections,” in *ICCV*, 2015, pp. 3862–3870.
- [26] A. Oliva and A. Torralba, “Modeling the shape of the scene: A holistic representation of the spatial envelope,” *International Journal of Computer Vision*, vol. 42, no. 3, pp. 145–175, 2001.
- [27] J. Philbin, O. Chum, M. Isard, J. Sivic, and A. Zisserman, “Object retrieval with large vocabularies and fast spatial matching,” in *CVPR*, 2007.
- [28] —, “Lost in quantization: Improving particular object retrieval in large scale image databases,” in *CVPR*, 2008.
- [29] E. Ristani, F. Solera, R. Zou, R. Cucchiara, and C. Tomasi, “Performance measures and a data set for multi-target, multi-camera tracking,” in *ECCV workshop on Benchmarking Multi-Target Tracking*, 2016.

- [30] S. Shafer, A. Stentz, and C. Thorpe, "An architecture for sensor fusion in a mobile robot," in *ICRA*, vol. 3, 1986, pp. 2002–2011.
- [31] Y. Sun, L. Zheng, Y. Yang, Q. Tian, and S. Wang, "Beyond part models: Person retrieval with refined part pooling," *CoRR*, vol. abs/1711.09349, 2017. [Online]. Available: <http://arxiv.org/abs/1711.09349>
- [32] C. Szegedy, V. Vanhoucke, S. Ioffe, J. Shlens, and Z. Wojna, "Rethinking the inception architecture for computer vision," in *CVPR*, 2016, pp. 2818–2826.
- [33] O. R. Terrades, E. Valveny, and S. Tabbone, "Optimal classifier fusion in a non-bayesian probabilistic framework," *IEEE Trans. Pattern Anal. Mach. Intell.*, vol. 31, no. 9, pp. 1630–1644, 2009.
- [34] Q. Tian, N. Sebe, M. S. Lew, E. Loupas, and T. S. Huang, "Content-based image retrieval using wavelet-based salient points," in *Storage and Retrieval for Media Databases 2001, San Jose, CA, USA, January 24, 2001*, 2001, pp. 425–436.
- [35] G. Toliás, R. Sircé, and H. Jégou, "Particular object retrieval with integral max-pooling of CNN activations," *CoRR*, vol. abs/1511.05879, 2015. [Online]. Available: <http://arxiv.org/abs/1511.05879>
- [36] M. Wang, H. Li, D. Tao, K. Lu, and X. Wu, "Multimodal graph-based reranking for web image search," *IEEE Trans. Image Processing*, vol. 21, no. 11, pp. 4649–4661, 2012.
- [37] L. Wei, S. Zhang, H. Yao, W. Gao, and Q. Tian, "GLAD: global-local-alignment descriptor for pedestrian retrieval," in *ACM MM*, 2017, pp. 420–428.
- [38] C. Wengert, M. Douze, and H. Jégou, "Bag-of-colors for improved image search," in *ACM MM*, 2011, pp. 1437–1440.
- [39] J. Wright, A. Y. Yang, A. Ganesh, S. S. Sastry, and Y. Ma, "Robust face recognition via sparse representation," *IEEE Trans. Pattern Anal. Mach. Intell.*, vol. 31, no. 2, pp. 210–227, 2009.
- [40] J. Yang, J.-y. Yang, D. Zhang, and J.-f. Lu, "Feature fusion: parallel strategy vs. serial strategy," *Pattern recognition*, vol. 36, no. 6, pp. 1369–1381, 2003.
- [41] H. Yao, S. Zhang, Y. Zhang, J. Li, and Q. Tian, "Deep representation learning with part loss for person re-identification," *CoRR*, vol. abs/1707.00798, 2017. [Online]. Available: <http://arxiv.org/abs/1707.00798>
- [42] D. Yi, Z. Lei, S. Liao, and S. Z. Li, "Learning face representation from scratch," *CoRR*, vol. abs/1411.7923, 2014. [Online]. Available: <http://arxiv.org/abs/1411.7923>
- [43] K. Zhang, Z. Zhang, Z. Li, and Y. Qiao, "Joint face detection and alignment using multitask cascaded convolutional networks," *IEEE Signal Processing Letters*, vol. 23, no. 10, pp. 1499–1503, Oct 2016.
- [44] N. Zhang, M. Paluri, Y. Taigman, R. Fergus, and L. D. Bourdev, "Beyond frontal faces: Improving person recognition using multiple cues," in *CVPR*, 2015, pp. 4804–4813.
- [45] S. Zhang, M. Yang, T. Cour, K. Yu, and D. N. Metaxas, "Query specific fusion for image retrieval," in *ECCV*, 2012, pp. 660–673.
- [46] S. Zhang, M. Yang, X. Wang, Y. Lin, and Q. Tian, "Semantic-aware co-indexing for near-duplicate image retrieval," in *ICCV*, 2013.
- [47] L. Zheng, L. Shen, L. Tian, S. Wang, J. Wang, and Q. Tian, "Scalable person re-identification: A benchmark," in *ICCV*, 2015.
- [48] L. Zheng, S. Wang, Z. Liu, and Q. Tian, "Lp-norm IDF for large scale image search," in *CVPR*, 2013, pp. 1626–1633.
- [49] —, "Packing and padding: Coupled multi-index for accurate image retrieval," in *CVPR*, 2014, pp. 1947–1954.
- [50] Z. Zheng, L. Zheng, and Y. Yang, "Unlabeled samples generated by gan improve the person re-identification baseline in vitro," in *ICCV*, 2017.



identification.

Liang Zheng is a Lecturer and a Computer Science Futures Fellow in the Research School of Computer Science, Australian National University. He received the Ph.D degree in Electronic Engineering from Tsinghua University, China, in 2015, and the B.E. degree in Life Science from Tsinghua University, China, in 2010. He was a postdoc researcher in the Center for Artificial Intelligence, University of Technology Sydney, Australia. His research interests include image retrieval, classification, and person re-



current research interests include image processing, computer vision, video surveillance, and pattern recognition. He is a member of the IEEE and the IEICE.

Shengjin Wang received the B.E. degree from Tsinghua University, China, in 1985 and the Ph.D. degree from the Tokyo Institute of Technology, Tokyo, Japan, in 1997. From 1997 to 2003, he was a member of Research Staff in the Internet System Research Laboratories, NEC Corporation, Japan. Since 2003, he has been a Professor with the Department of Electronic Engineering, Tsinghua University. He has published over 80 papers on image processing, computer vision, and pattern recognition.



Zhongdao Wang received his B.S degree in the Department of Physics at Tsinghua University in 2017. He is now working towards the Ph.D. degree in the Department of Electronic Engineering at Tsinghua University. His research interests include computer vision, pattern recognition and particularly person/face recognition and retrieval.